JOURNAL OF GEOPHYSICAL RESEARCH, VOL. 101, NO. D15, PAGES 20,909–20,924, SEPTEMBER 20, 1996

Development of the Antarctic ozone hole

Mark R. Schoeberl,[1] Anne R. Douglass,[1] S. Randolph Kawa,[1] Andrew E. Dessler,[1] Paul A. Newman,[1] Richard S. Stolarski,[1] Aidan E. Roche,[2] Joe W. Waters,[3] and James M. Russell III[4]

Abstract. A Lagrangian chemical model is used to simulate the formation of the Antarctic "ozone hole": the decrease in high-latitude southern hemisphere ozone between mid-August and mid-September of each year. The model benchmark simulation of HNO_3, $ClONO_2$, ClO, and ozone for September 17, 1992, is in good agreement with UARS observations. Simulations of the ozone column over the years 1979–1994 show quantitative agreement with the secular decline in Antarctic ozone and change in the area of the ozone hole as observed by the total ozone mapping spectrometer (TOMS). The model calculates that the Antarctic ozone loss and ozone hole area both increased linearly with time after the early 1970s until the early 1990s. After the early 1990s the growth of the area of the ozone hole slows as a result of the slowing of the growth rate of total inorganic chlorine. A hypothetical doubling of the 1992 atmospheric chlorine amount would expand the ozone hole to the very edge of the polar vortex.

1. Introduction

The key processes associated with Antarctic ozone depletion have been identified [*Solomon*, 1990; *Anderson et al.*, 1991; *McElroy*, 1992; *World Meteorological Organization* (*WMO*), 1989, 1991, 1995]. During the austral winter, polar stratospheric clouds (PSCs) form in the lower stratosphere due to the cold temperatures found there. While there is some uncertainty as to the exact composition and formation temperature of the clouds, it is known that the effects of these clouds occur at temperatures below ~196 K and lead to almost complete conversion of total inorganic chlorine (Cl_y) from its primary reservoir species HCl and $ClONO_2$ into the labile species Cl_2 and HOCl [*Kawa et al.*, 1996]. When sunlight returns to the region in the spring, these labile species are photolyzed and lead to the formation of the ClO radical. Catalytic ozone loss occurs through the ClO + ClO dimer mechanism [*Molina and Molina*, 1987] and the ClO + BrO mechanism [*McElroy et al.*, 1986] and leads to the removal of virtually 100% of the ozone between 14 and 20 km. This loss of ozone reduces the column abundance of ozone by 50 to 70% and has become known as the "ozone hole." A key factor in the formation of the ozone hole is the meteorological isolation of the Antarctic region [*Schoeberl et al.*, 1991; *Bowman*, 1993; *Chen*, 1994], without which atmospheric mixing would dilute the ozone loss [e.g., *Anderson et al.*, 1991].

While individual chemical and dynamical aspects of the ozone hole have been studied in detail, the integrated phenomenon has not been quantitatively simulated. The only type of model currently capable of simulating the ozone hole is the two-dimensional model. Two-dimensional model simulations, however, generally fail to reproduce the ozone hole due to the low spatial resolution of the models, inadequate vertical descent within the simulated fall vortex, the failure to sufficiently isolate the polar vortex, and the complexities associated with parameterizing heterogeneous chemistry [e.g., *Brasseur*, 1993]. With the availability of constituent data from the Upper Atmosphere Research Satellite (UARS) and stratospheric wind data from National Meteorological Center (NMC), we attempt in this paper to quantitatively simulate the Antarctic ozone hole using a Lagrangian chemical model. Our study will focus on the evolution of Antarctic ozone on three isentropic levels: 400, 440, and 500 K, which bracket the bulk of Antarctic stratospheric ozone. By combining the ozone simulated on these levels with microwave limb sounder (MLS) ozone profiles at higher potential temperature surfaces, the column ozone change over the integrating period can be simulated. Comparisons with total ozone mapping spectrometer (TOMS) column ozone and MLS profile ozone observations are used to test the validity of the model. Finally, by adjusting the model stratospheric chlorine, we can compare the model estimates of column ozone changes to compare with the historical TOMS record back to 1980.

In section 2 we briefly discuss the model and the chemical initialization procedure. We then compare the model simulation of 1992 with 1992 UARS data to evaluate the model. We then discuss our simulations of the Antarctic hole from 1970 to 1999. A subsequent section describes the model sensitivities to dehydration, denitrification, and doubling chlorine. Conclusions are presented in section 7.

2. Lagrangian Chemical Model

To simulate the Antarctic ozone hole for a given year, we set 625 parcels on each of three potential temperature surfaces: the 400-, 440-, and 500-K surfaces, corresponding approximately to 15- to 20-km altitude. The parcels are initialized on a regular grid throughout the middle- and high-latitude southern hemisphere on September 17 of the year being simulated. The parcels are advected backward in time until August 17 on isentropic air parcel trajectories. The chemical composition of each parcel on August 17 is then initialized using the UARS

[1]NASA Goddard Space Flight Center, Greenbelt, Maryland.
[2]Lockheed Palo Alto Research Laboratory, Palo Alto, California.
[3]Jet Propulsion Laboratory, Pasadena, California.
[4]NASA Langley Research Center, Hampton, Virginia.

Paper number 96JD01707.
0148-0227/96/96JD-01707$09.00

data from mid-August 1992. These parcels are subsequently advected forward in time back to September 17, at which point they again lie on the regular grid on which they were initialized. At each time step of the forward advection (15 min) a chemistry box model updates the chemical composition of each parcel using the parcel's latitude, longitude (hence solar zenith angle), pressure, and temperature for that time step. The chemical box model is an improved version of the model used by *Kawa et al.* [1993] and *Douglass et al.* [1995]. Improvements include updated gas phase reaction and photolysis rates reported by *DeMore et al.* [1994], a new chemical integrator, a fast table look-up photolysis scheme, and heterogeneous reactions as discussed by *Kawa et al.* [1995]. The trajectory model is described by *Schoeberl and Sparling* [1995], and we use NMC-balanced winds [*Newman et al.*, 1988] for this study.

The time period of August 17 to September 17, 1992, is determined by the UARS orbit and instrument operational period. This time frame brackets the time period of a UARS yaw cycle in 1992 when UARS observed the high-latitude southern hemisphere. In addition, the cryogenic limb array etalon spectrometer (CLAES) operated from shortly after launch in September 1991 until its cryogen was exhausted in May 1993. Thus there are CLAES observations of $ClONO_2$ and HNO_3 for the austral winter of 1992 only. This period also covers the time of most rapid Antarctic ozone loss according to column ozone data [*WMO*, 1991, Figure 2-1; *Newman et al.*, 1991; *Stolarski et al.*, 1986].

The type of Lagrangian chemical model has been used in the past to study the chemistry of both the Arctic and the Antarctic regions [e.g., *Jones et al.*, 1989; *Schoeberl et al.*, 1993a; *Kawa et al.*, 1993, 1995]. The Antarctic winter stratospheric conditions are particularly suited for this simple approach since (1) the diabatic descent rates during the late Antarctic winter are very low [*Schoeberl et al.*, 1991, 1995; *Rosenfield et al.*, 1994; *Manney et al.*, 1995a], with typical values of the heating rates being 0.1 to 0.2 K/d [*Rosenfield et al.*, 1994] and (2) the Antarctic lower stratosphere is already denitrified. Thus to first order, the aerosol sedimentation processes which denitrify the Antarctic stratosphere have already taken place and are implicit in the initialization.

Model Initialization

As mentioned previously, the parcels of the Lagrangian chemical model are initialized on August 17 of the year being simulated with mid-August UARS data. Version 7 data from the UARS CLAES, version 17 data from the Halogen Occultation Experiment (HALOE), and version 3 data from the microwave limb sounder (MLS) instruments are used. Validation papers for the various instruments and constituents can be found in a special issue of the *Journal of Geophysical Research*, volume 101, 1996.

To set the initial chemical composition of the parcels, we use August 17, 1992, MLS and CLAES data interpolated to potential temperature surfaces and averaged as a function of modified potential vorticity (MPV) [*Lait*, 1994]. The potential temperature and MPV make up a two-dimensional coordinate system, with potential temperature the "vertical" coordinate and MPV the "horizontal" coordinate. Once the trace gas field is determined as a function of potential temperature and MPV, the same functional form is used to initialize the system in the simulations of the other years. Thus we are assuming that the relationship of the constituents to the potential temperature and MPV fields is the same for each year with the exception of the chlorine containing gases, which are adjusted for the growth in inorganic chlorine (described below). This methodology follows the PV reconstruction system developed by *Schoeberl and Lait* [1992] and used by *Redaelli* [1994].

Figures 1a–1g show the August 17, 1992, 440-K observations and the fit to MPV. Note that the HCl data were collected between July 18 and August 17, 1992 Figure 1h shows the relationship between MPV and latitude on August 17. Note that the lowest MPV values computed are above −3.4 units. Separate MPV fits are also performed at 400 K and 500 K potential temperatures (not shown). The thin lines in the figure show an average of the UARS data. The thick lines show the fit used in the model, and these lines mostly overlay the averages of the data, obscuring the thin lines except in parts of Figures 1d and 1e. For $ClONO_2$ and HNO_3 measured by CLAES the cold vortex temperatures and the presence of aerosols generate some retrieval problems deep within the vortex so the fits are adjusted as shown. The deep vortex adjustments are based on the trends in the data as MPV decreases.

The vortex edge is located near MPV = -1.5×10^5 K m^2/kg/s (about 60°S) from the edge determining algorithm described by *Nash et al.* [1996]. The inner edge of the vortex, also determined by the Nash et al. algorithm, is located at MPV = -2.3×10^5 K m^2/kg/s (about 65°S). This is roughly where HNO_3 (Figure 1e), $ClONO_2$ (Figure 1d), and H_2O (Figure 1g) begin to decrease rapidly with more negative MPV and is sometimes referred to as the chemically processed region (CPR) [*Proffitt et al.*, 1989]. These measurements confirm that the Antarctic vortex is already dehydrated and denitrified and allows us to neglect the processes of dehydration and denitrification in the model. Both of these processes would be difficult to parameterize since precipitation of condensates involves cross-isentropic transport.

Figure 1b shows N_2O derived from measurements of CH_4 by the HALOE using the linear relationship between these two trace gases [*Prather and Remsberg*, 1993]. N_2O is directly measured by the CLAES, but the cold temperatures in the polar vortices make the retrievals in the vortex unreliable. Aircraft N_2O observations [*Loewenstein et al.*, 1989] are in reasonable agreement with N_2O derived from HALOE CH_4. Thus we will use the N_2O derived from HALOE.

HALOE HCl observations (Figure 1c) for the month prior to the initialization of the model on August 17 do not sweep far enough south to penetrate the vortex. The HCl fit for MPV < -1.8×10^5 K m^2/kg/s is determined from later HALOE HCl observations [*Douglass et al.*, 1995]. Since $ClONO_2$ also decreases poleward within the vortex, the HCl measurements suggest that the dominant chlorine species is ClO or the dimer Cl_2O_2. This is consistent with the analysis of aircraft data [*Kawa et al.*, 1992] and is confirmed by MLS measurements as will be shown below.

We can use the HCl and $ClONO_2$ information to initialize the ClO abundance instead of using MLS ClO which has strong diurnal variability. We set ClO to be the difference between Cl_y (discussed below) and HCl plus $ClONO_2$. As it turns out, our model calculations are insensitive to the initial amounts of ClO because the heterogeneous chemistry in the vortex adjusts the partitioning of the chlorine system with a timescale of days.

HNO_3 is initialized from CLAES measurements as shown in Figure 1e. Ozone is initialized from MLS measurements shown in Figure 1f. Both HNO_3 and ozone estimates show Figure 1e

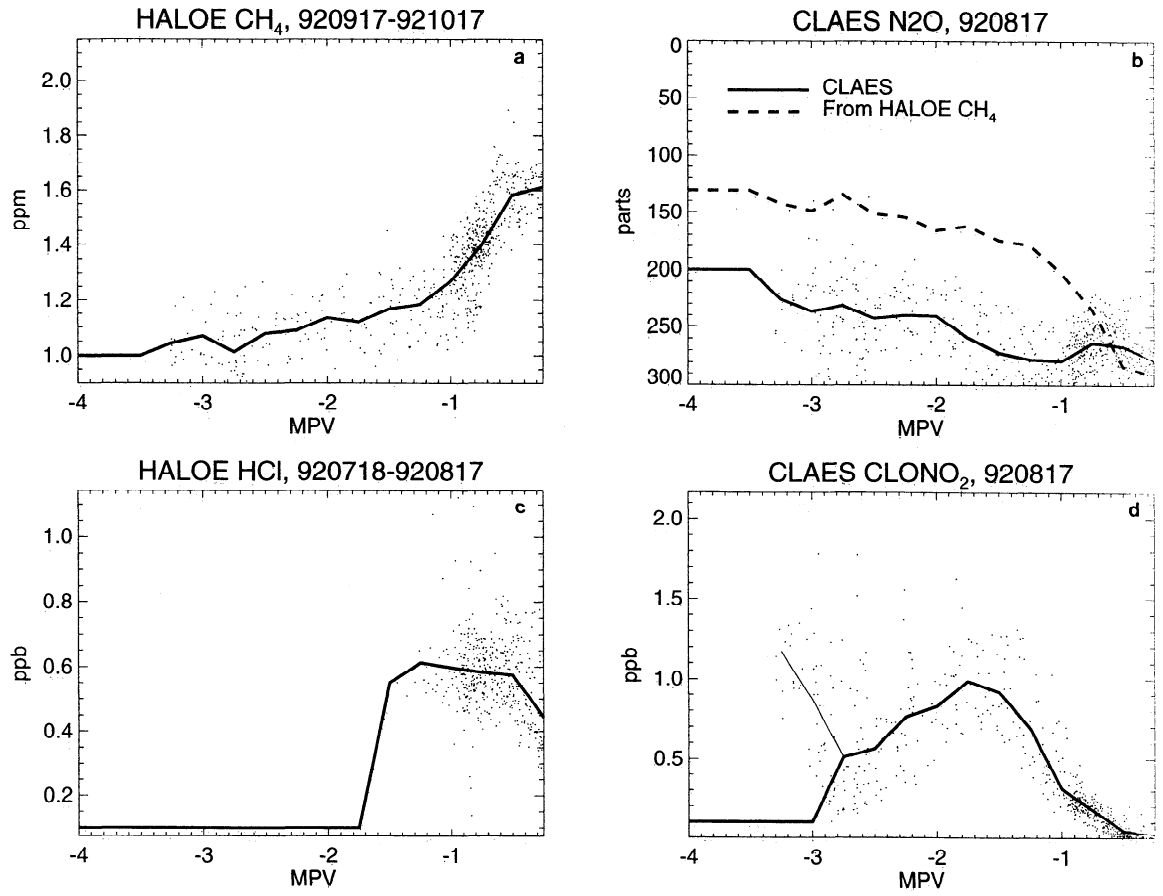

Figure 1. UARS observations as a function of modified potential vorticity (MPV) used to initiate the Lagrangian chemical model on the 440-K potential temperature surface. The small dots indicate the data, the thin line (mostly under the thick line) shows the fit to the data, while thick lines show the fit used to initialize the Lagrangian model. (The thick line usually overlays the thin line except for low MPV values.) Titles indicate the UARS instrument from which the data are derived and the date range of the data (for HALOE) in the YYMMDD format (YY is the year, MM is the month number, DD is the day of the month). The units of MPV are 10^5 K m^2/kg/s. (a) HALOE methane data taken over the period indicated. (b) CLAES N_2O and N_2O derived from HALOE CH_4 using the relation between the two long-lived tracers derived from aircraft data [*Prather and Remsberg*, 1993]. (c–g) Trace gases as indicated. (h) MPV as a function of latitude on the 440-K surface; the vertical lines indicate the range of MPV on a latitude circle.

and 1f are consistent with the aircraft estimates of *Fahey et al.* [1989] and *Proffitt et al.* [1989].

Water vapor is initialized from MLS observations shown in Figure 1g. The MLS water vapor mixing ratios at the edge and exterior of the vortex (Figure 1g) are higher than recorded by 1987 aircraft observations [*Kelly et al.*, 1989] and by the HALOE for the period September 16 to October 5, 1992. For example, the HALOE measurements show average water vapor amounts of about 4 parts per million by volume (ppmv) at 440 K except poleward of the vortex edge where water vapor amounts drop to an average of 3 ppmv. In contrast, the MLS water vapor data show vortex exterior amounts of 6 ppmv dropping to a value below 2 inside the vortex (Figure 1g). The uncertainty in water vapor affects PSC (ice and nitric acid trihydrate (NAT)) formation temperatures, as is discussed farther below.

Total inorganic chlorine (Cl_y) for a given year is derived from N_2O concentration from a fit to N_2O following the procedure of *Woodbridge et al.* [1995]. First, an estimate of total chlorine (organic plus inorganic) is determined from (11) of Woodbridge et al. using total tropospheric chlorine and growth rate of total tropospheric chlorine (determined over the previous five years) from the *WMO* [1995, 1989]. Total organic chlorine is calculated from the equation in the caption of Figure 3 of Woodbridge et al. This equation is based on 1992 data, so to account for the changing chlorine content in the atmosphere, we multiply the equation by the ratio TC/3670, where TC is the total tropospheric chlorine for the year being simulated in parts per trillion by volume and 3670 pptv is the total tropospheric chlorine in 1992. Cl_y is the difference between total chlorine and total organic chlorine. The N_2O fit allows for the conversion of organic chlorine to inorganic chlorine as the stratospheric air parcel ages.

Figure 2 shows the Cl_y used in our model. Note that there is little total inorganic chlorine increase after 1995. Our MPV fits for the members of Cl_y (HCl and $ClONO_2$) shown in Figure 1 are based on 1992 measurements. To initialize parcels in years other than 1992 (which have different Cl_y), we scale the 1992 HCl and $ClONO_2$ fits by the ratio TC/3670. Note that as $ClONO_2$ changes with Cl_y, HNO_3 is adjusted so that total NO_y is the same in all years.

The parcels are initialized with sulfate aerosol surface area

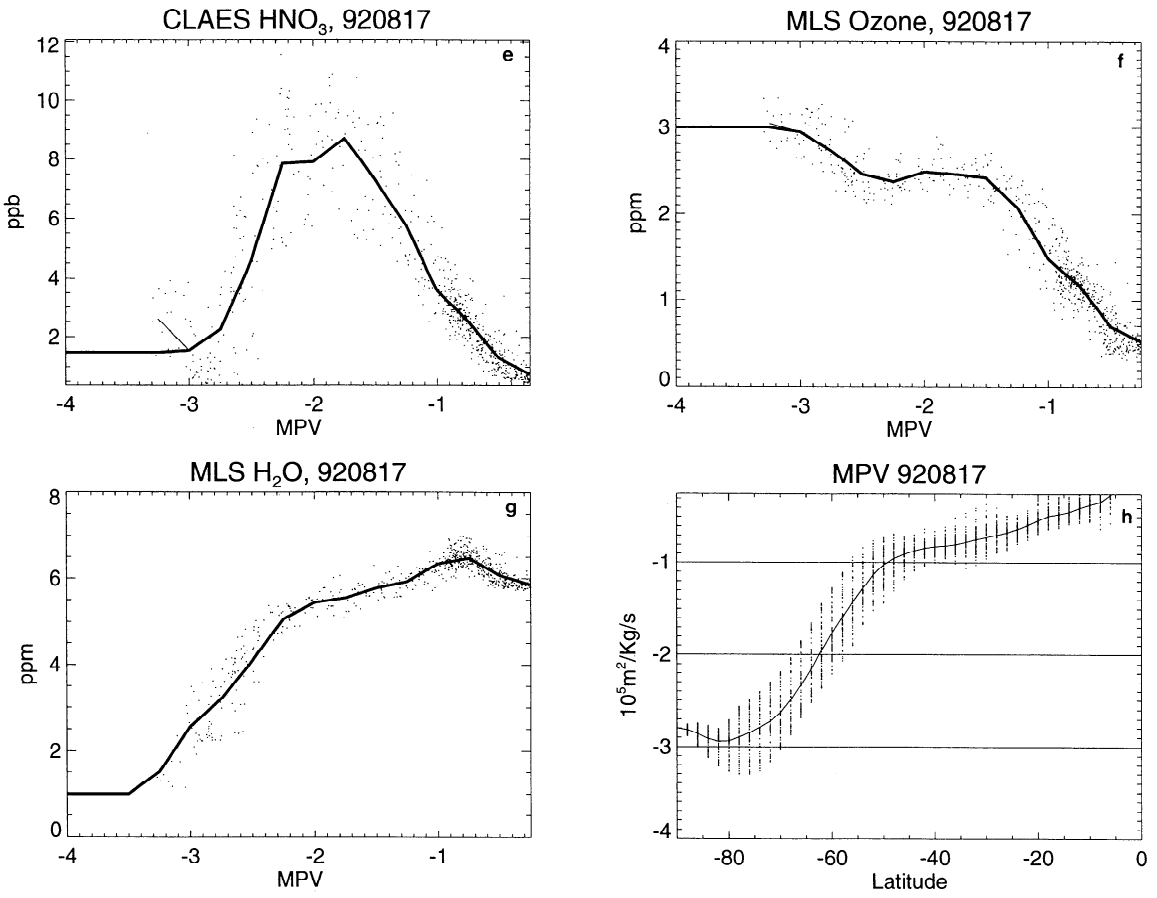

Figure 1. (continued)

from *WMO* [1991, Table 8-8]. For 1992 and 1993 we use SAGE II data [*Thomason and Poole*, 1995] to account for the enhancement in surface area due to the Mount Pinatubo eruption. Heterogeneous reaction rates on sulfate are parameterized according to the formulation of *Hansen and Ravishankara* [1994]. Volcanic aerosols are assumed to be unimportant inside the vortex during this period because heterogeneous chemistry on PSCs will overwhelm heterogeneous effects on sulfate aerosols. Br_y is set at 15 pptv.

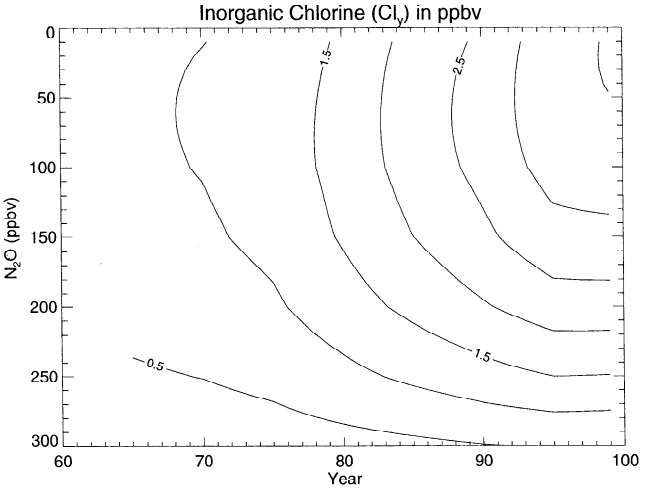

Figure 2. The secular increase in Cl_y from *WMO* [1989, 1995] combined with N_2O data fit from *Woodbridge et al.* [1995].

Sample Trajectory

Figure 3 shows the chemical history of a trajectory from August 17 to September 17, 1992. This trajectory was initialized with differing amounts of HCl to test the sensitivity of the model to the chlorine initialization. The location of this air parcel is initially near the outer edge of the vortex (MPV = -2.5×10^5 K m^2/kg/s) although it moves to slightly lower MPV values by the end of the integration. Initially, the excess ClO from the initialization scheme recombines with NO_2 to form $ClONO_2$ leading to a drop in ClO and quick rise in $ClONO_2$. Heterogeneous processing takes place shortly after day 235 when the temperature of the parcel falls below the nitric acid trihydrate (NAT) formation temperature (top right-hand panel). At that temperature the chemical model initiates heterogeneous reactions. HCl and $ClONO_2$ concentrations drop with a rapid rise in reactive chlorine (ClO + $2Cl_2O_2$) concentrations. Nitric acid amounts also increase slightly. These heterogeneous processes have been observed in the laboratory [see *DeMore et al.*, 1994] and indirectly confirmed by the aircraft observations [*Toohey et al.*, 1993; *Schoeberl et al.*, 1993a, b; *Webster et al.*, 1993; *Kawa et al.*, 1995]. After the processing event, reactive chlorine concentrations begin to slowly decrease, and the $ClONO_2$ concentrations begin to increase as HNO_3 photolysis produces NO_2 which recombines with ClO [*Schoeberl et al.*, 1993a]. The HCl concentration also increases as Cl reacts with methane. The weak oscillations in the reactive

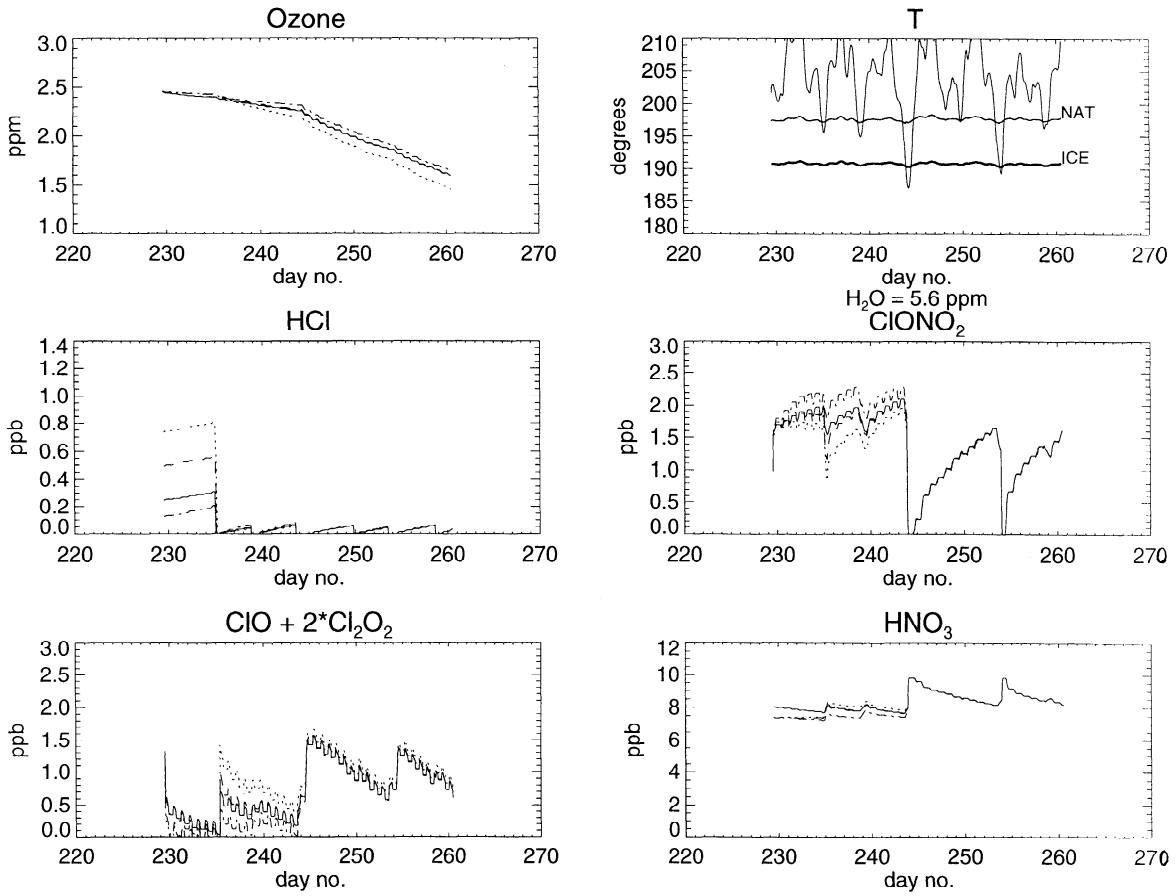

Figure 3. The constituent history of a parcel using different initial HCl concentrations. Chemical constituents are shown as labeled. Normal HCl initialization is indicated by the solid line. Other HCl values, 0.5, 2, and 3 times "normal" are given by dashed-triple dotted, dashed, and dotted lines, respectively. Top right-hand panel shows parcel temperature, the nitric acid trihydrate formation temperature (NAT) and frost point temperature (ICE) computed from HNO_3 and water amount. Water is conserved in each parcel; the mixing ratio is given underneath the top right panel. The integration period is August 17 to September 17, 1992.

chlorine and $ClONO_2$ concentrations are due to daytime photolysis with nighttime recombination of the products.

The subsequent processing event on day 239 has a smaller affect on the abundance of the chlorine species since HCl is nearly depleted. On day 244 the parcel is exposed to ice temperatures which triggers the reaction $ClONO_2 + H_2O \rightarrow HOCl + HNO_3$. The chlorine nitrate concentration falls to zero with reactive chlorine and nitric acid increasing rapidly. $ClONO_2$ begins to recover until a second ice event on day 254. Overall, ozone loss in this parcel is significant especially following the ice processing events which greatly elevate the reactive chlorine.

To show that the HCl initialization scheme has little impact on the overall ozone loss, the parcel was initialized with half, twice, and 3 times the HCl amount and the computation was repeated. Prior to the ice event, the excess HCl gives rise to higher amounts of ClO. This generates small differences in ozone loss up to the ice event. After the ice event, all chlorine is thrown into Cl_X; both HCl and $ClONO_2$ are near zero. Since Cl_y was conserved in this experiment, the model shows no significant differences after the ice event.

At midlatitudes, for the potential temperature values used here, the model will reach its own equilibrium after about 20 days with 10% of the Cl_y as $ClONO_2$ and 90% in HCl regardless of the initial values of HCl and $ClONO_2$. This partitioning is consistent with the aircraft data analysis of *Stimpfle et al.* [1994], which suggested that about 88% of the Cl_y is in HCl, and the analysis by *Dessler et al.* [1995], which showed that the UARS data are broadly consistent with two-dimensional model estimates of the reservoir chlorine partitioning.

3. Comparison With UARS Data

The Lagrangian chemistry model is run for 31 days using 625 parcels distributed from 30°S to the pole. The parcels are first set up on a regular grid and run backward in time. The regular grid of parcels is shown in Plate 1 (top middle). After the backward integration on the 440-K surface using 1992 winds, the parcels form an irregular field shown in Plate 1 (top left). The chemical model is then initialized using the MPV-trace gas relationships (Figure 1) and run forward along the parcel back trajectories.

Plates 1 and 2 compare model chemical species with UARS observations for the same dates. The UARS data are interpolated to the 440-K potential temperature surface and averaged into 4° latitude by 10° longitude bins. The trajectory points are averaged in the same manner for plotting except for the ozone fields which are averaged into 20° longitude by 4° latitude bins.

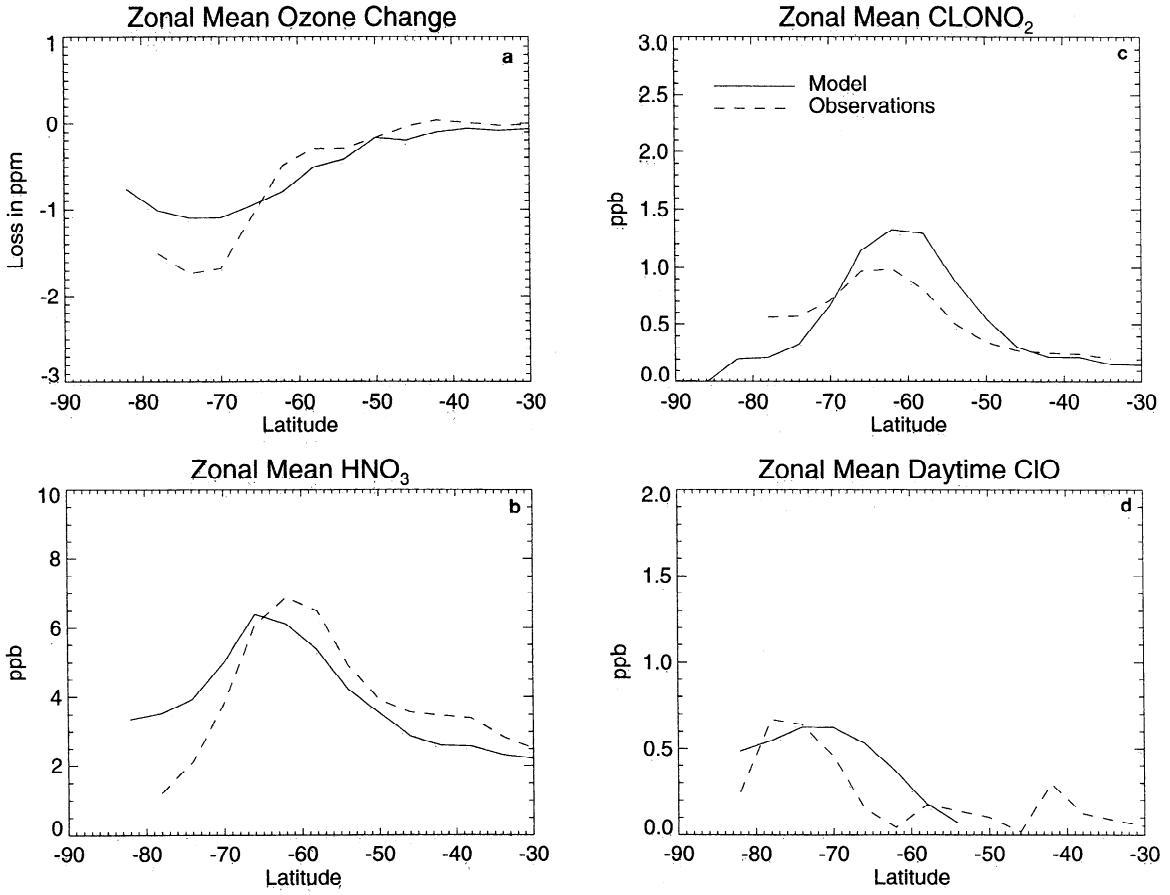

Figure 4. (a) Zonal mean ozone, (b) HNO_3, (c) $ClONO_2$, and (d) daytime ClO amounts (solid line) compared with UARS observations (dashed line) for September 17, 1995. Ozone and ClO observations are from MLS; HNO_3 and $ClONO_2$ are from CLAES. Values below 0.1 ppbv in the model ClO are not plotted.

The larger averaging bins are needed to compute differential ozone loss over the 1-month period since the August 17 parcel distribution is not uniform. Gaps appear where there are too few trajectory points in the irregular field.

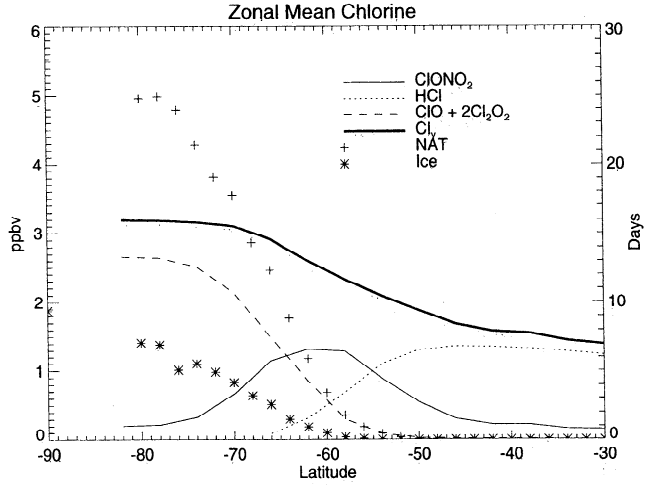

Figure 5. Comparison of zonal mean trace gas amounts from the model on September 17 as indicated on the figure. The zonal mean total number of days the parcels are exposed to temperatures below nitric acid trihydrate condensation point and frost point are also shown.

Plate 1 (right, top, and bottom) compares the change in ozone. The left-hand figures show that the MPV initialization procedure has produced slightly more model ozone than MLS observations. The final model ozone (middle) is in good agreement with MLS observations. There does appear to be slightly more ozone loss at high southern latitudes in the model than appears in the observations. Differences between the initial model and the final model ozone show that the model ozone depletion region is somewhat larger than observed. The model integrations also show that the ozone loss maximizes in a ring near 70°S which is consistent with MLS observations for this period [*Manney et al.*, 1993].

Plate 2 compares the model on September 17, 1992, with various UARS constituents on that same day. CLAES measurements of $ClONO_2$ and model $ClONO_2$ (left) both show elevated $ClONO_2$ in a collar or ring aligned with the edge of the vortex, i.e., the collar region, a phenomenon first noted by *Toon et al.* [1989]. The agreement between the CLAES observations and the model are generally good, but the model $ClONO_2$ has a slightly higher mixing ratio. Model nitric acid (center) also shows the ring and compares well with CLAES HNO_3 observations. In both cases, the lower resolution of the UARS data as averaged into the data bins may be responsible for the broader feature. Model HCl (top right) shows that heterogeneous conversion of HCl occurs over the entire vortex region. HCl values have fallen below the small initialization value (Figure 1c) within the vortex. The MPV map (bottom

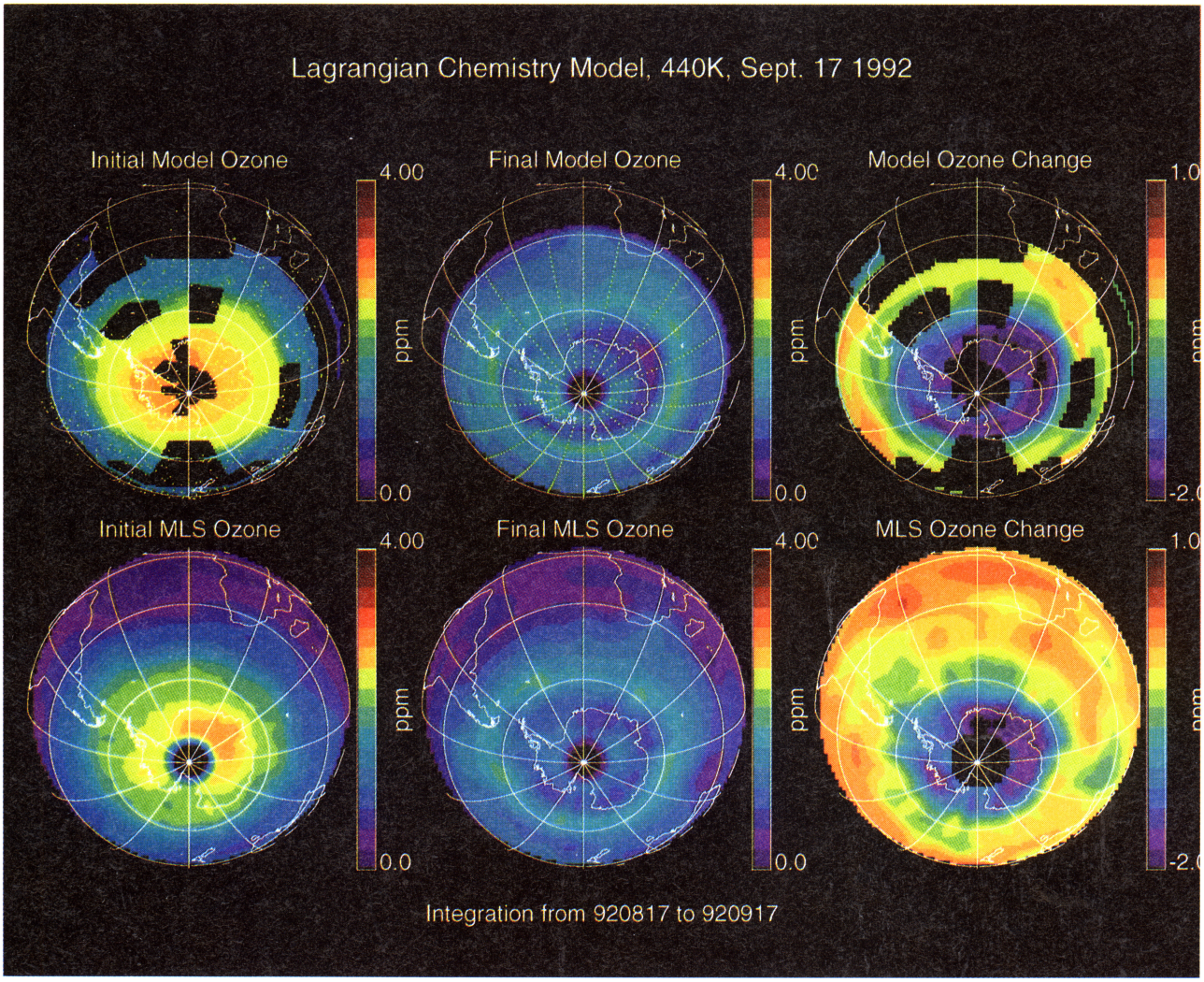

Plate 1. Changes in ozone at 440 K from August 17 to September 17, 1992. Top panels show model results; bottom panels, MLS observations. Top left and middle figures also show the parcel distribution (yellow dots). Units as indicated.

right) shows that there have been no significant intrusions of midlatitude air into the vortex.

In general, the model makes only small changes in the distribution of the chlorine reservoir species during this period. This is an expected result since the chlorine partitioning of the Antarctic system should already have been set by the heterogeneous reactions prior to initialization.

To obtain a more quantitative comparison between the model and the observations, in Figure 4a we compare zonal averages of model output on September 17, 1992, with zonal averages of UARS data on September 17, 1992. Day-night averages are used for ozone, $ClONO_2$, and HNO_3. For ClO, only daytime averages are used. ClO observations are also adjusted as recommended by *Waters et al.* [1996].

The zonal mean ozone change between August 17 and September 17, 1992 (Figure 4a) shows the largest decrease near 70°S consistent with MLS observations (see Plate 1). However, in the vortex the model generates about 0.6 ppmv smaller loss than is observed. Model nitric acid (Figure 4b) compares well with CLAES observations equatorward of the peak. Poleward of the peak, however, CLAES data show less nitric acid. This is probably due to continued denitrification in the Antarctic stratosphere since temperatures in the polar region are cold enough to form ice PSCs and precipitate HNO_3.

Model $ClONO_2$ (Figure 4c) is higher than CLAES observations equatorward of about 68°S but is lower than CLAES poleward of 68°S. Comparing Figures 4b and 4c we see that the model probably has shifted NO_y into $ClONO_2$ from HNO_3 equatorward of 68°S. Poleward of 68°S, the excess HNO_3 in the model is probably producing more NO_2 which increases $ClONO_2$ concentrations slightly.

Daytime zonal mean ClO levels (Figure 4d) are in good agreement with MLS observations on September 17, but the model underestimates ozone loss. One possible explanation is that there is more inner vortex mixing in the model than occurs in the atmosphere as a result of trajectory errors associated with the meteorology [see *Morris et al.*, 1995]. Examining the conservation of MPV shows that there is more parcel mixing than expected if MPV is strictly conserved. Since the heterogeneous chemistry associated with PSC encounters is constantly "resetting" the chlorine system, this mixing would not be evident in the chlorine species but would smooth out the zonal mean ozone loss. Close examination of Figures 6a and 4

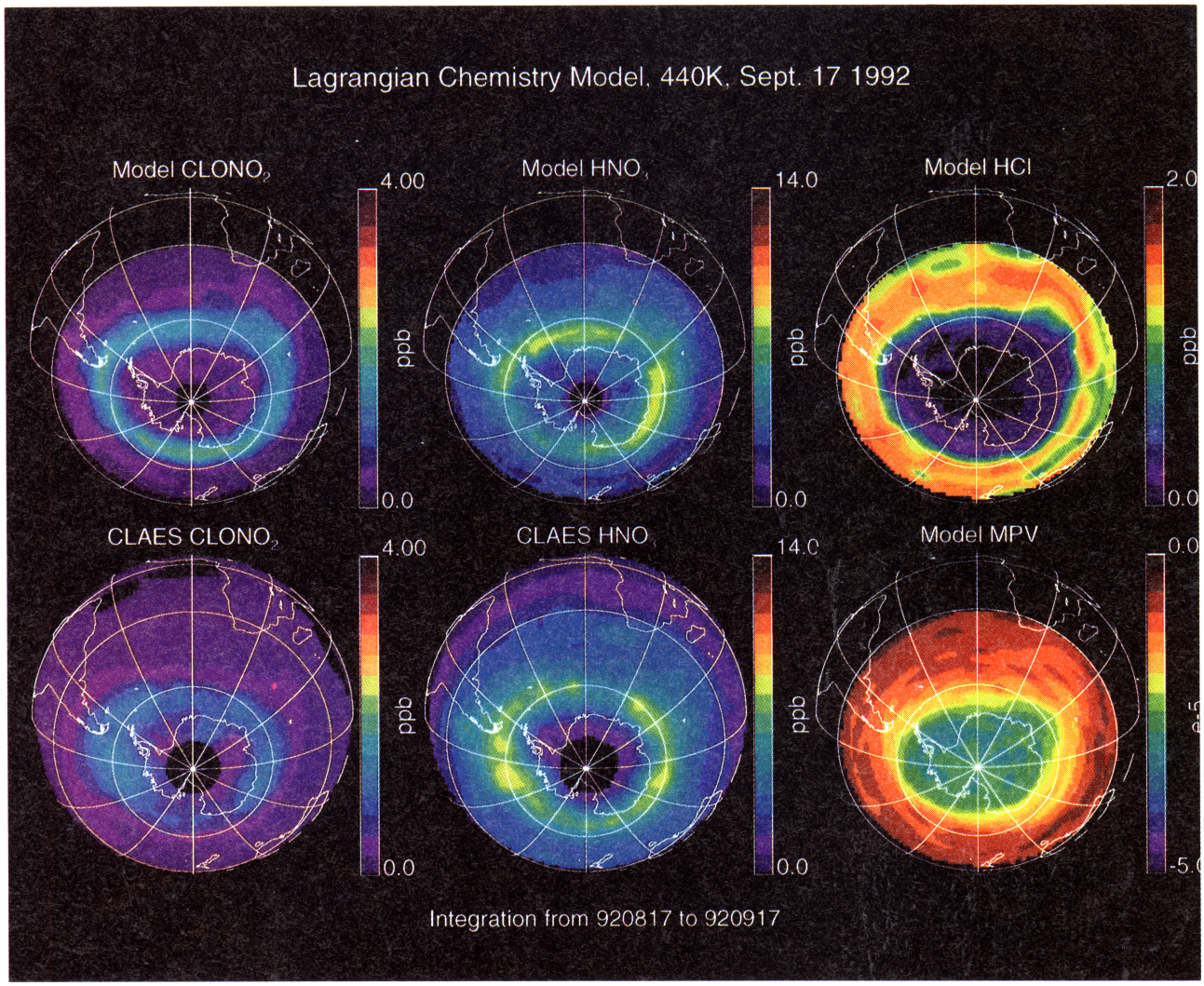

Plate 2. Model trace gas comparisons with UARS data as in Plate 1. Left figures show modeled and CLAES $ClONO_2$; middle panels show modeled and CLAES HNO_3; right panels show HCl and MPV. All fields are shown at the end of the integration period (September 17).

suggests a wider (more mixed) ozone hole in the model than observations suggest.

We can use the model to show the relationship between the chlorine species and structure of the ozone hole as summarized in Figure 5. HCl loss serves as a marker of the edge of the chemically processed vortex [*Webster et al.*, 1993], corresponding to the most equatorward region of PSC formation temperatures. Cl_y is significantly higher in the vortex than midlatitude Cl_y because air in the vortex has descended from higher altitudes where organic chlorine has been photolyzed.

Figure 1d shows that the model is initialized with enhanced $ClONO_2$ near the edge of the vortex. Plate 2 and Figure 5 show that $ClONO_2$ is still enhanced by the end of the integration period. Although the model does not denitrify, the frequent heterogeneous processing at ice temperatures prevents the rise of $ClONO_2$ deep in the vortex. The collar locates a condition where temperatures are cold enough for heterogeneous reactions to occur but not cold enough for frequent ice processing. At this time of year, there is sufficient sunlight and HNO_3 to produce enough NO_2 so that $ClONO_2$ stays elevated in the collar and ClO is low relative to higher latitudes. The recovery of HCl from its low initial conditions is suppressed within the vortex by occasional processing on NAT or liquid aerosol particles. The chemistry of this region of the Antarctic vortex during this time period is similar to the Arctic vortex because denitrification is not prevalent.

At higher southern latitudes, Figure 5 shows that $ClONO_2$ and HCl have small concentrations. The majority of Cl_y is in the form of ClO and Cl_2O_2. This inner vortex zone is defined by frequent exposure of the air parcels to ice temperatures (asterisks in Figure 5). The formation of ice particles followed by their sedimentation leads to the removal of NO_y, which is principally made up of HNO_3, from the vortex. This denitrification defines the boundary of the CPR and removes the deactivation pathway for reactive chlorine, which is the reaction between ClO and NO_2 and allows ClO to remain enhanced for days or weeks.

4. Simulating Column Ozone Loss

Most of the historical record of ozone loss is contained in the Antarctic ground-based and total ozone mapping spectrometer (TOMS) satellite data. The data are summarized in *WMO* [1989, 1991]. It is unlikely that calculations on a single isen-

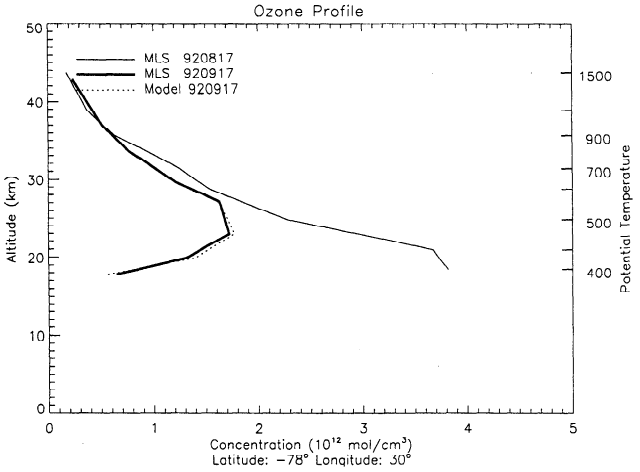

Figure 6. Comparison of ozone profiles from the model and MLS as 78°S and 30°E. Thin solid line shows the MLS observations averaged into a 4° latitude by 10° longitude bins for August 17, 1992. The thick solid line shows the observations for September 17, 1992. Model results for September 17 are attached to September profile (dotted line) and are indicated in the legend as MLS*. The potential temperature levels used in the calculation are shown as tick marks on the right axis.

tropic level will be adequate to simulate the column ozone loss. Thus we apply the model at three separate isentropic levels 500, 440, and 400 K which approximately correspond to 17, 19, and 22 km, respectively. These altitudes cover the core of the Antarctic ozone depletion region [*WMO*, 1989; Figure 1.1.5-1; *Hofmann et al.*, 1989].

Figure 6 shows typical MLS ozone profiles taken at the beginning and at the end of the model integration period (August 17 to September 17). The MLS data have been interpolated onto the isentropic surfaces 400, 440, 500, 600, 800, 1100, and 1500 K levels (the last four are approximately 25, 30, 36, and 42 km, respectively) then horizontally averaged into 10° longitude by 2° latitude bins. To compare the model results with observations, model values of ozone at the end of the integration period are substituted into the 400-, 440-, and 500-K potential temperature surfaces. These potential temperature surfaces account for about 160 Dobson units (DU) out of roughly 250 DU column ozone present in mid-August. Furthermore, the largest Antarctic ozone changes occur below 32 km. This is consistent with the findings of *Manney et al.* [1995b] who estimated the Antarctic vortex transport of ozone from a diabatic trajectory calculation and compared it to MLS observations. Their calculations showed that chemical ozone loss must be occurring up to 30 km; the loss was balanced by downward diabatic transport of ozone. Manney et al. showed that near 500 K and below, the diabatic replenishment of ozone could be neglected during this period, and most of the ozone is lost through chemical processes. Model calculations compared with observations for individual profiles show excellent agreement. A typical example is shown in Figure 6.

Integrating the ozone profiles (as in Figure 6) we can produce a surrogate column ozone map using the model. Plate 3 shows maps of TOMS column ozone, column ozone computed from integrating the MLS profiles, and column ozone amounts after inserting the initial and final model ozone values at 400, 440, and 500 K into the MLS profiles. We will refer to the latter as model-modified MLS data. This procedure neglects the contribution of tropospheric ozone (10–30 DU), but MLS and lidar ozone comparisons show that MLS slightly overestimates the ozone amounts (R. D. McPeters, personal communication). The overestimate produces an excess in the MLS column ozone that tends to compensate for the neglect of tropospheric ozone in the column integration. This compensating effect should not change significantly over the years. Plate 3 shows that the integrated MLS and model-modified MLS column ozone amounts are in overall agreement with TOMS observations between 65°S and 30°S. Poleward of 65°S, there is some disagreement on the column ozone amounts in August with the August 17 TOMS data showing lower ozone compared to integrated MLS.

Figure 7 compares the zonal mean total ozone values from TOMS and MLS. For August 17 the difference between MLS integrated ozone and TOMS is about 60 DU. For mid-September the agreement is quite good, but as indicated above, TOMS is underestimating column ozone amounts relative to MLS. One factor which could lead to the mid-August discrepancy is the possibility of ozone loss at lower levels (below 440 K) before mid-August where MLS retrievals are less sensitive to ozone amounts. The lower August TOMS ozone may also be a result of a transient ozone minihole event present during this period. *Newman et al.* [1988], *McKenna et al.* [1989] and *Peters et al.* [1995] show that tropopause uplift associated with these synoptic scale features produce anomalously low column ozone amounts. The uplift produces high clouds and often stratospheric PSCs. The magnitude of the ozone minihole is often exaggerated further because TOMS tends to underestimate the column ozone in the presence of high clouds at high solar zenith angles [*Torres et al.*, 1992].

To summarize Plate 3 and Figure 7, by substituting three model levels (400, 440, and 500 K) into the MLS ozone profiles, we are able to reasonably reproduce the observed column ozone changes. This suggests that our model realistically reproduces the mechanism responsible for the ozone loss at this time of year. We are now ready to examine the secular changes in ozone due to chlorine increase.

5. Secular Changes in Antarctic Ozone

Since the chemistry and dynamics in the Lagrangian model are separable, the Cl_y amounts can be varied for each year (see Figure 2) while still using the NMC winds and temperature fields for that year, or the wind and temperature fields from different years can be used. In the studies below we use 1992 dynamics as a baseline. There were no significant lower-stratospheric warmings in 1992, and the parcel trajectories are largely zonal for the integration period. TOMS observations over the late winter, spring period show significant column ozone loss [*Herman et al.*, 1995].

We first examine the model response at 440 K to the secular chlorine increase from 1980 to the present using 1992 NMC winds and temperature fields. Figure 8a shows the 440 K ozone loss, $ClONO_2$, ClO, and HCl as total chlorine increases for each year. The systematic rise in HCl, $ClONO_2$, and ClO are apparent; HNO_3 (not shown) decreases slightly as NO_y is shifted from HNO_3 to $ClONO_2$. Coincident with the 30% rise in ClO, the model produces a doubling of the ozone loss. This nonlinear response of the system is expected from the quadratic dependence of the ClO dimer ozone loss mechanism on ClO abundance [*Molina and Molina*, 1987]. Figure 8a also

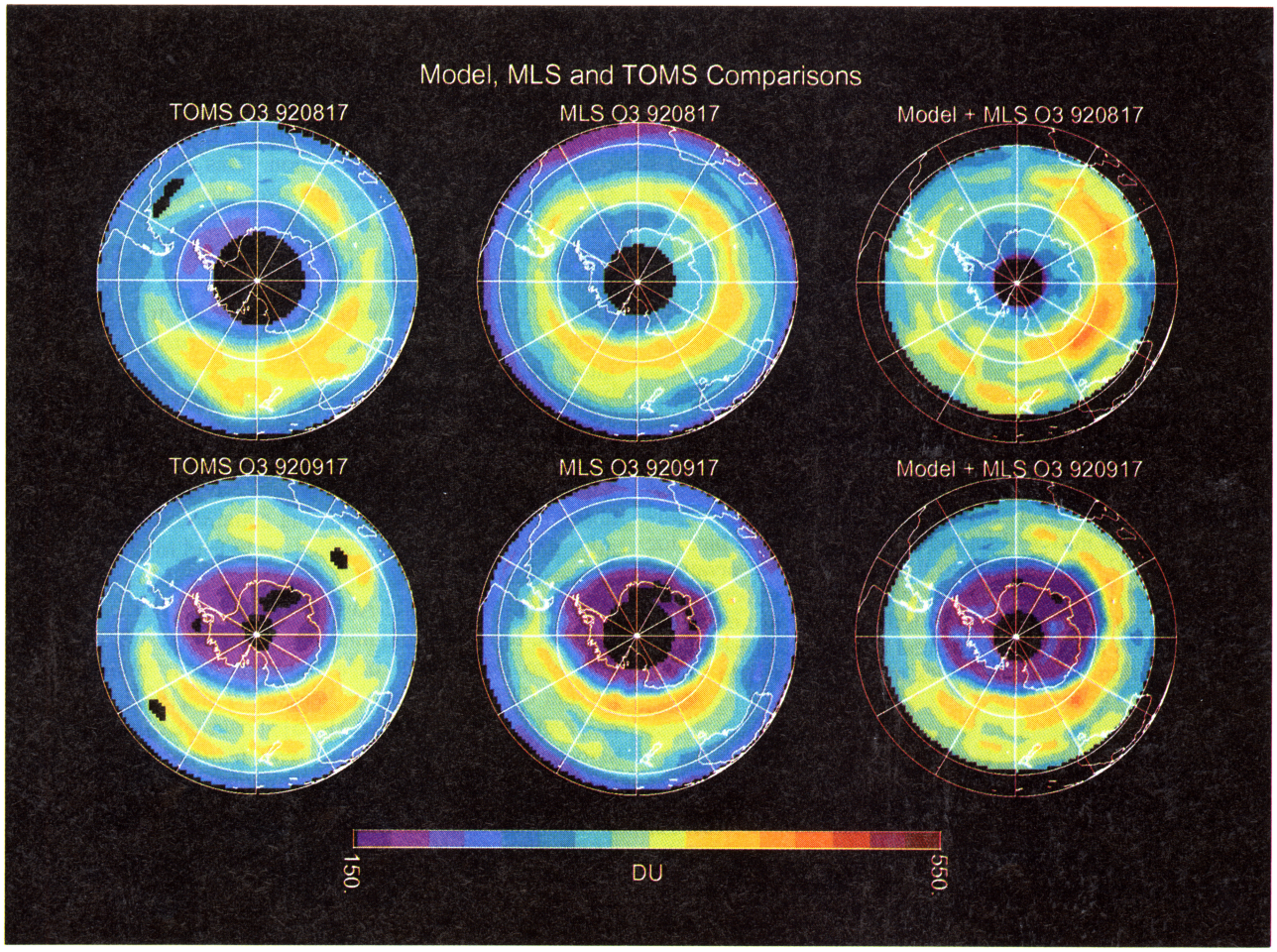

Plate 3. Total ozone maps from TOMS (left), integrating MLS (middle), and integrating MLS with model levels at 400, 440, and 500 K inserted into the profiles. Units are Dobson units.

shows that the ozone loss tends to slow in the late 1990s. This occurs because the growth of inorganic chlorine slows (Figure 2).

Figure 8b shows the results at 400 K. At this potential temperature, the ozone mixing ratio is significantly lower than at 500 and 440 K. In addition, HCl is higher than $ClONO_2$ in 1980. Increases in Cl_y thus show up mostly as increases in HCl. Thus processing events tend to deplete $ClONO_2$. As HCl increases over the years, $ClONO_2$ drops, as is seen in the figure. However, this does not explain the dramatic increase in HCl seen in the late 1980s. Note that initially, ClO increases as Cl_y increases. But by the late 1980s, about 95% of the ozone has been lost by the end of the integration period. When the ozone is gone, the partitioning between Cl and ClO shifts to Cl, leading to the conversion of ClO, Cl_2O_2, and $ClONO_2$ into HCl as Cl reacts with methane. Thus Figure 8b shows, paradoxically, that the increases in Cl_y during the 1990s lead to decreases in ClO and $ClONO_2$, with the increase in Cl_y going into HCl. This shift in Cl_y from ClO and $ClONO_2$ into HCl, first predicted by *Prather and Jaffe* [1990], has been observed in the Antarctic at 460 K by UARS HALOE [*Douglass et al.*, 1995].

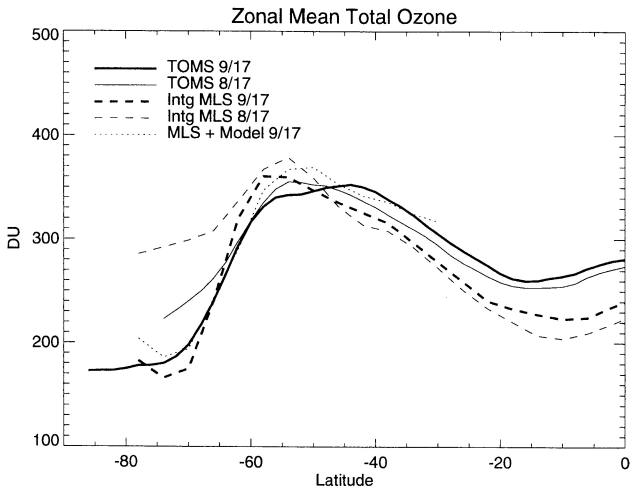

Figure 7. Zonal mean total ozone values from TOMS (solid lines), integrated MLS (dashed lines) for August 17, 1992, and September 17, 1992, and integrated MLS ozone substituting in model calculations for September 17 shown as the dotted line.

Figure 9 shows average ozone loss inside the vortex (MPV < -1.5) at 440, 500, and 400 K as a function of year. The 440 K calculations are extended to the mid-1960s; the dynamics are the same as 1992 (solid circles). The pluses show the cases where the dynamics for the appropriate year are used at 440 K. The extremely quiet vortex conditions for 1992 are dramatically illustrated in this figure with the 440 K DYY curve lying completely above the 440 K D92 curve.

The 1992 dynamics cases shown in Figure 9 at 440 K show a

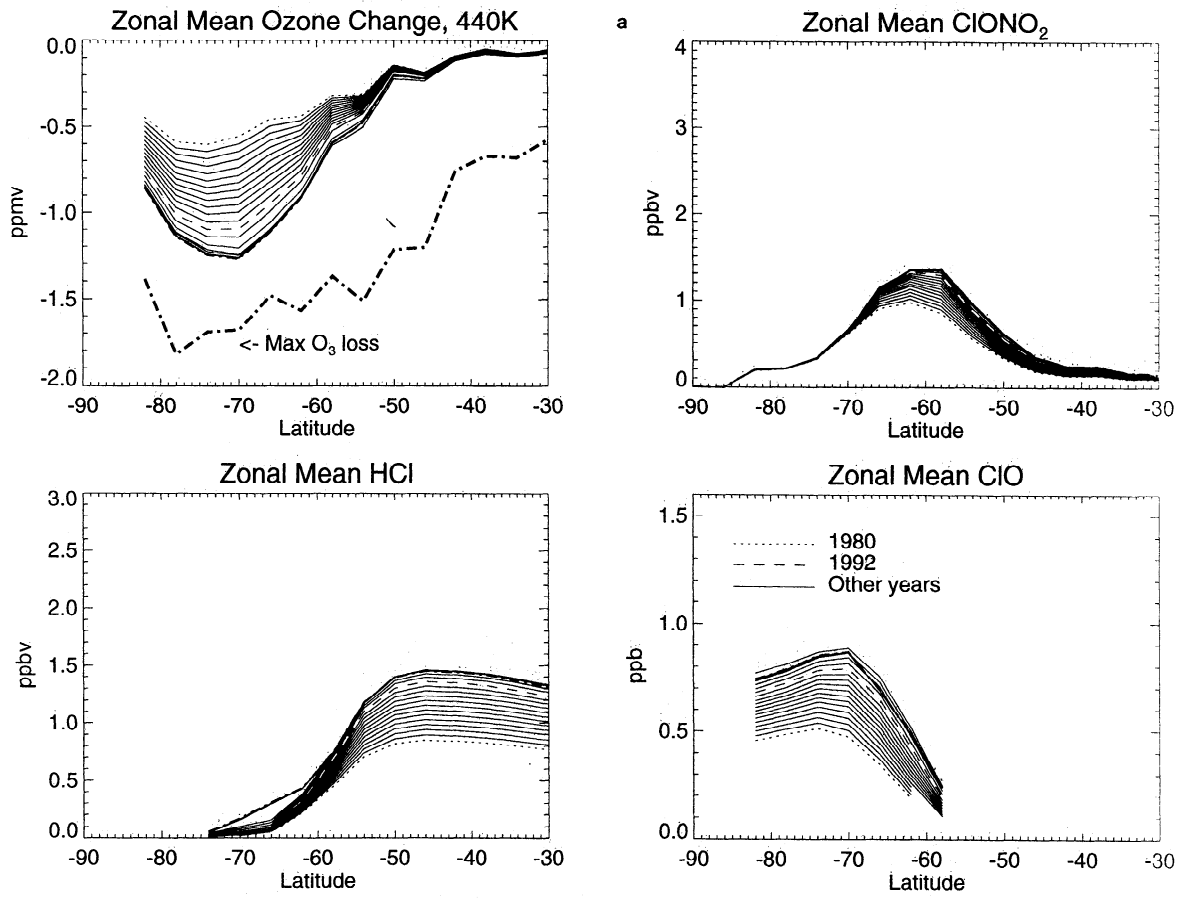

Figure 8. The sequential changes in Antarctic ozone, $ClONO_2$, HCl, and ClO as total chlorine is increased from 1980 to 1999. The thin lines show each year; the bold dashed line is 1992 in each panel; the dotted line is 1980. The thick solid line in the top left panel is the maximum ozone loss (negative of the August 17 ozone amount). The 1992 NMC wind fields are used for each of the integrations. (a) 440 K; (b) 400 K.

slow decline in Antarctic ozone during the late 1960s, followed by a more rapid almost linear decline up to the early 1990s. After 1994–1995, ozone loss appears to flatten out at 440 and 500 K. The 1994–1995 change coincides with the leveling off of the stratospheric chlorine increase (Figure 2). At 400 K, ozone loss tapers off before chlorine growth slows consistent with the saturation of the system shown in Figure 11b.

Including the year-to-year dynamical variability at 440 K reduces ozone loss (Figure 9). The system is apparently sensitive to dynamical variability, but our simulation of the observed ozone loss variability is not quantitatively consistent with observations. To show this, Figure 10 compares the September 17 TOMS polar minimum ozone amounts and area extent of the ozone hole with the model-modified MLS amounts for each year. We simulate the overall linear decline in the Antarctic total ozone reasonably well, although the model has failed to reproduce low minima for 1986, 1987, and 1993 and has underestimated the minima for 1981 and 1984.

As a further diagnostic, the bottom panel of Figure 10 compares the computation of the model change in the ozone hole area with the TOMS ozone hole area, both as defined by 220 DU contour. Also shown is the September 17 area of the 440 K polar vortex as averaged over the years 1980–1995. The model column ozone values are computed using MLS 1992 ozone profiles for the levels above 500 K (see Figure 6). The vortex area is defined by the MPV region interior to the maximum MPV gradient [*Nash et al.*, 1996]. The model reproduces the area and the overall change in the area of the ozone hole fairly well. Note that the dynamically quiet year of 1992 provides a maximum with respect to observations for the area change. Note also that the area of the ozone hole has not reached the average area of the vortex.

As expected from the asymptotic behavior shown in Figure 9, Figure 10 shows that the model predicts a slowing in the growth of the ozone hole area and minimum value in the late 1990s. Likewise, the September 17 minimum total ozone value approaches about 110 DU. This asymptotic behavior is in response to a slowing of the growth in chlorine (Figure 2).

The results shown in Figure 10 also indicate that the overall year-to-year decline in ozone observed by TOMS is well reproduced, although we are unable to reproduce the exact year-to-year variability. Part of this problem may be associated with the initial conditions. Our study assumes that ozone observed in 1992 will have the same functional relationship with MPV for all other years. Although we have verified this assumption for the years 1992–1994, we cannot show that the functional relationship does not have more year-to-year variability in the 1980s. A more certain source of error is that associated with the month-long trajectory integrations and with the quality of the meteorological data sets for the Antarctic region. Note that the model is able to reproduce the magnitude of year-to-year variability observed in Antarctic ozone loss. *Morris et al.* [1995]

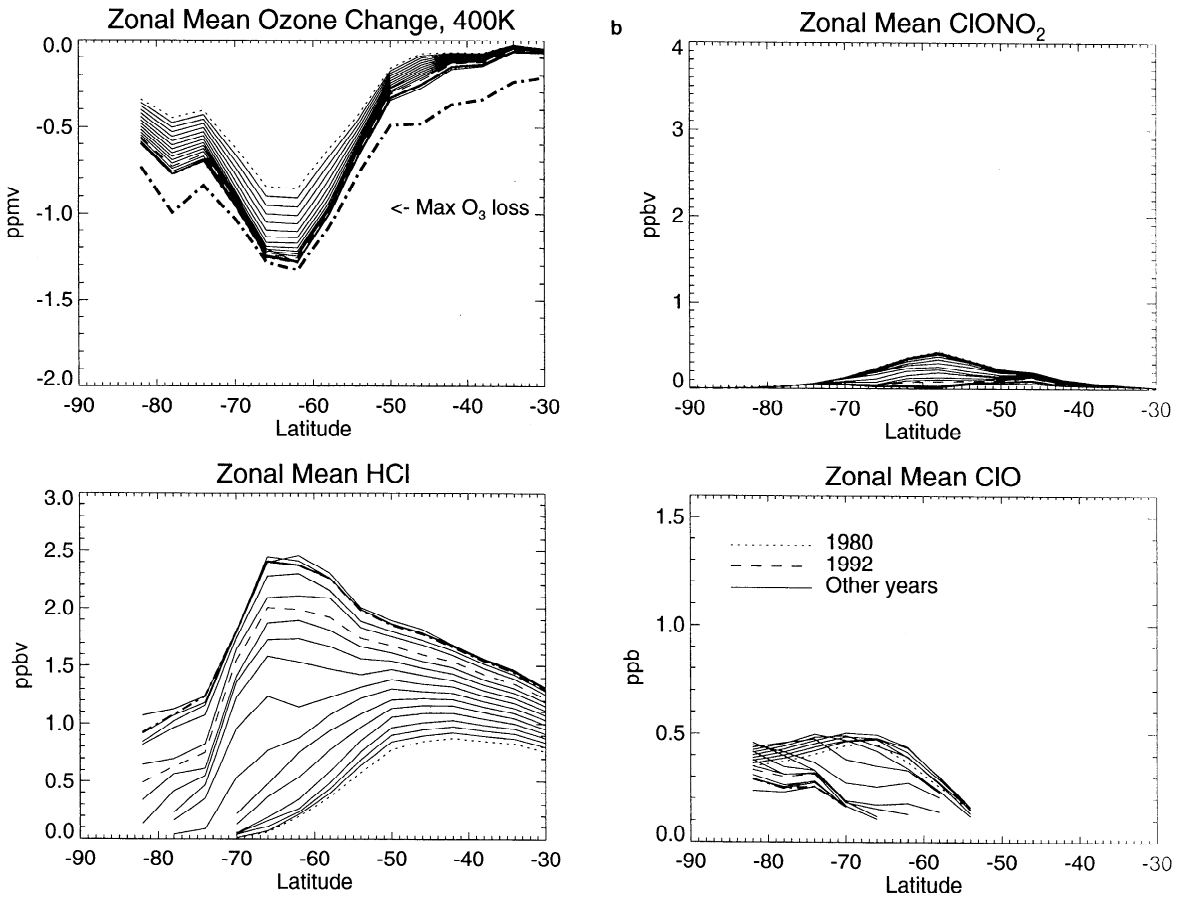

Figure 8. (continued)

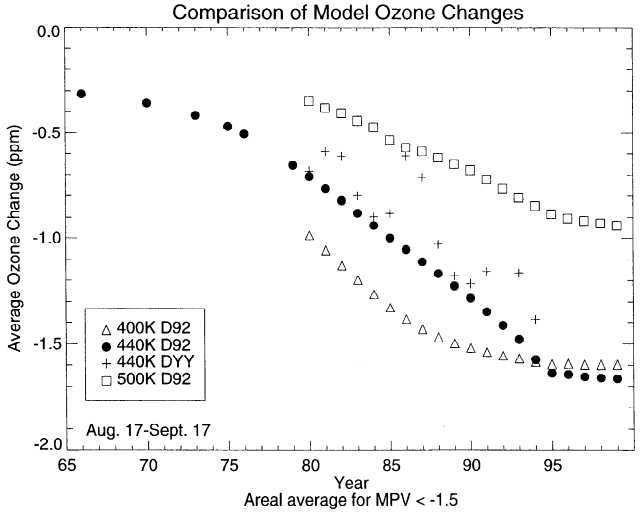

Figure 9. Average ozone changes from August 17 to September 17 for each year within the Antarctic vortex. Circles show secular changes in ozone at 440 K averaged over the vortex (MPV $< -1.5 \times 10^5$ K m^2/kg/s); the dynamics is taken to be the same as 1992. Squares and triangles shows the results at 400 and 500 K, respectively. Pluses show the results using the NMC-balanced wind data from that year to move the parcels (rather than 1992 balanced wind fields).

have pointed out that trajectory models are usually able to simulate the overall characteristics of an air mass for long integrations but are unable to simulate the exact air motion paths for periods longer than about 10 days. The trajectory approach here may thus be able to simulate the approximate climatology and magnitude of the year-to-year variability of the Antarctic ozone hole (from a meteorological viewpoint) while failing to simulate the details of a given year.

6. Model Sensitivity Experiments

Three additional 440 K experiments have been performed to examine the sensitivity of the polar chemical system to changes in water, NO_y, and chlorine. In the first case we examine the sensitivity of the model to the $ClONO_2$ hydrolysis reaction in maintaining high levels of ClO. The frequency at which the hydrolysis reaction occurs is strongly dependent on the frost point and hence is sensitive to the water vapor initialization. To examine the sensitivity to the initialization, we reduced the model water vapor amounts at 440 K to 2 ppbv everywhere. This has the effect of reducing the ice formation temperature. Figure 11 shows the results: Ozone loss is noticeably decreased, as is the concentration of ClO. Since the hydrolysis reaction is suppressed, $ClONO_2$ is expected to increase as indicated in the figure.

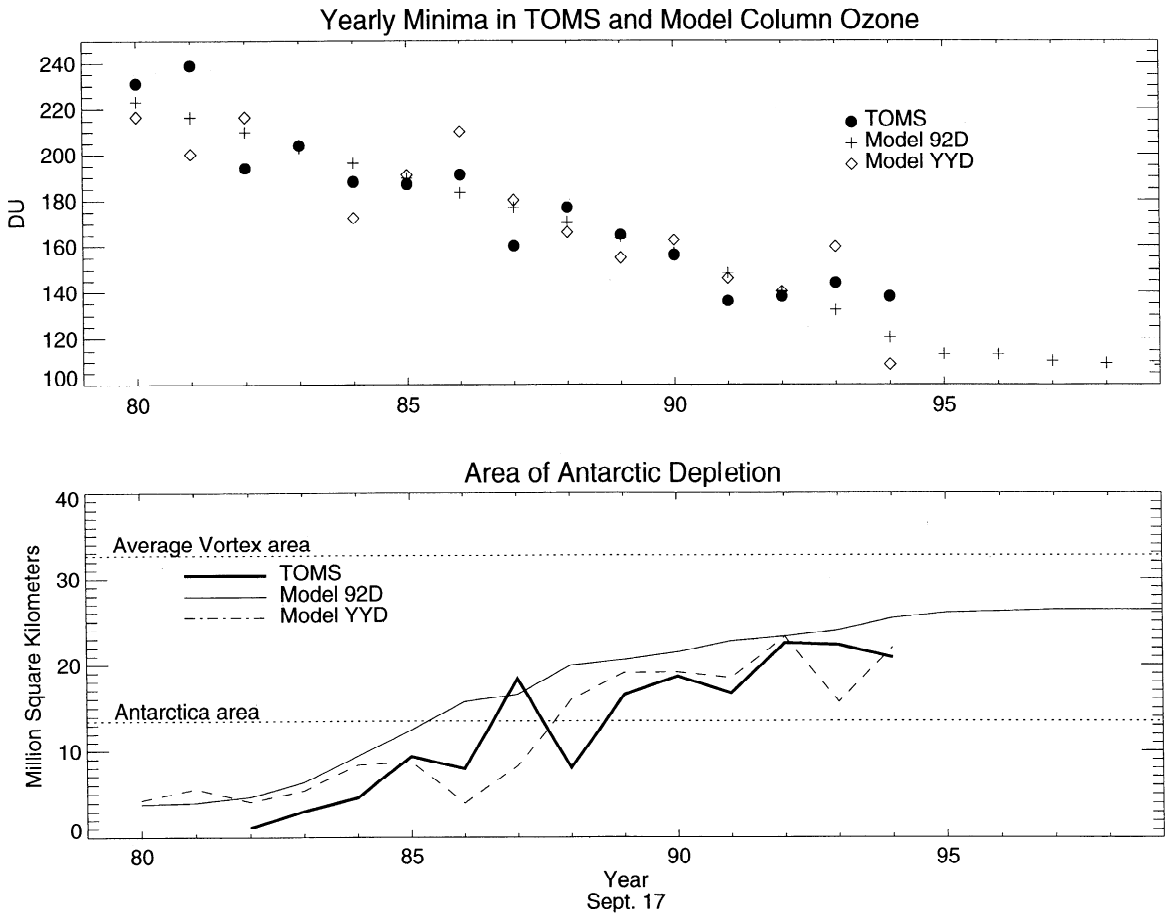

Figure 10. Comparison of TOMS minimum and model minimum column ozone amounts on September 17 for the year indicated (top figure). Model runs with 1992 dynamics (model 92D) are indicated by pluses. Bottom figure shows the area of the ozone depletion computed by the model, the model with 1992 dynamics, and TOMS. In all cases the area is the area of the polar region where total ozone is less than 220 DU. The average area of the polar vortex at 440 K over the same period is shown as a dotted line as is the area of the Antarctic continent.

In the natural polar stratosphere, water vapor is reduced by PSC sedimentation which also reduces NO_y. Thus the dehydrated stratosphere will also become denitrified [*Wofsy et al.*, 1990]. If NO_y levels remain low, then it will be difficult to reform $ClONO_2$ and ClO will remain high. Thus the denitrification which accompanies dehydration should reduce the sensitivity of the system to the amount of water vapor and ice formation. To test this, in addition to dehydrating the stratosphere, we reduce both NO_y and $ClONO_2$ within the vortex to 1.5 and 0.1 ppbv, respectively. Figure 11 shows that the ozone loss increases back toward the base calculation as expected. Thus despite the sensitivity of the system to initial water amounts, the system is not very sensitive to a consistent choice of dehydration and denitrification.

In the third experiment, stratospheric chlorine at 440 K is set at approximately twice the 1992 levels, corresponding to about 5.6 ppbv Cl_y at N_2O of 150 ppbv. The results in Figure 11 show that virtually all of the ozone has been destroyed within the vortex at this level and both $ClONO_2$ and ClO levels decrease, while HCl levels increase. This response is identical to that seen at 400 K for lower levels of chlorine. Plate 4 shows total column ozone from TOMS, the 1992 model-modified MLS data, and the doubled chlorine scenario model-modified MLS data. The ozone depletion in the doubled chlorine scenario is both deeper and covers a larger portion of the vortex than the 1992 model and TOMS data. The expansion of the area in the double chlorine scenario occurs because HCl remains high in the collar region of the vortex (Figure 11), so heterogeneous processing at the warmer (NAT) temperatures produce very high levels of ClO between 50°S and 60°S. The system is now like that shown in Figure 3 where HCl is tripled. The increases in collar ozone loss expands the ozone hole to the edge of the vortex. With the higher levels of $ClONO_2$ at midlatitudes, significant ozone changes occur there as well.

7. Summary

This study focuses on our ability to simulate the Antarctic ozone hole over the last 15 years. A Lagrangian chemical model, including a full suite of heterogeneous and gas phase chemical reactions and covering the southern polar stratosphere, is integrated over the period August 17 to September 17 for most years between 1966 and 1999. Observed and 1992 meteorological fields are used from 1980 to 1994; 1992 meteorological fields are used for the 1995–1999 and 1966–1979 integrations.

The major findings are (1) the model reproduces the general features of the chemical evolution of the Antarctic polar vor-

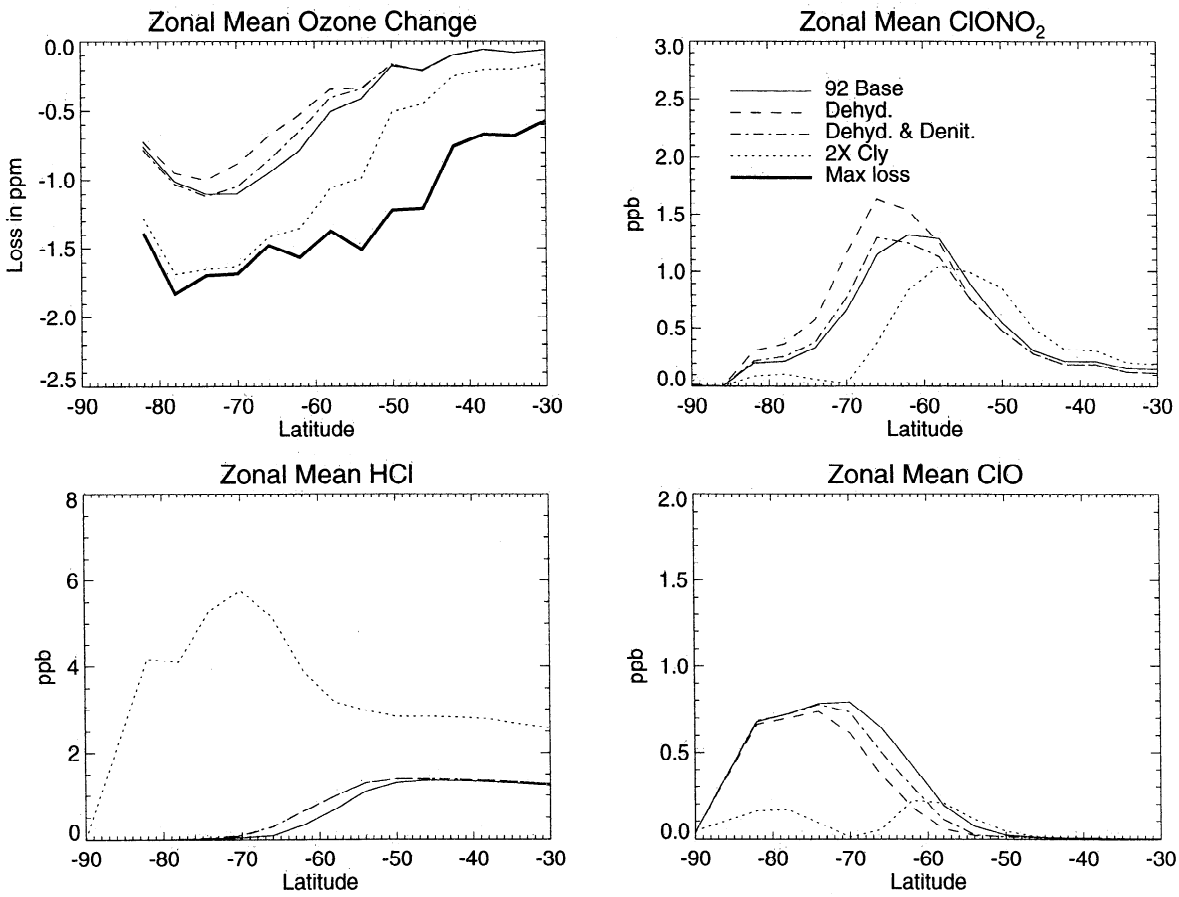

Figure 11. The results of uniformly reducing H_2O to 2 ppmv; reducing H_2O as before and, in addition, reducing HNO_3 to 1.5 ppbv and $ClONO_2$ to 0.1 ppbv inside the vortex; and doubling Cl_y from 1992 levels, and as in Figure 7. See text for details.

tex, including extensive ozone loss in 1992. The model and UARS measurements of ozone loss, ClO, $ClONO_2$, and HNO_3 on September 17 compare favorably. (2) Total column ozone changes over Antarctic have been simulated by substituting model calculations at the 400-, 440-, and 500-K isentropic surfaces into the MLS ozone profiles and integrating the column. Total ozone amounts computed in this manner are in agreement with both integrated MLS amounts and TOMS measurements for 1992. (3) Using estimates of changing stratospheric Cl_y and the NMC balanced wind climatology, we simulate the Antarctic ozone loss between 1965 and 1999. At 440 K the vortex averaged ozone loss during the August 17 to September 17 period began slowly in the late 1960s and early 1970s. Then from the late 1970s through the early 1990s, ozone loss increased steadily. During the late 1990s, ozone loss at 440 K is predicted to saturate. (4) The overall year-to-year decline in column ozone observed by TOMS is well reproduced by the model although we are unable to reproduce some of the year-to-year variability and details of the ozone hole structure. This inability is probably associated with the month-long trajectory integrations and with the quality of the dynamical data sets but is not critical since the overall secular decline in Antarctic ozone dominates the trend. (5) The model predicts that the current September 17 ozone hole size and minimum value have nearly stabilized. Up to the early 1990s, ozone loss was accelerating in the mid-August to mid-September period. The recent stabilization occurs because chlorine is no longer increasing rapidly in the lower stratosphere and ozone loss has saturated at the lowest levels. (6) Once the ozone is depleted, the model chlorine chemistry switches from a ClO-dominated system to a Cl-dominated system leading to rapid HCl formation. Ozone depletion is less complete at 440 K than at 400 K so the switch to rapid HCl formation can only occur later in the season at higher potential temperature surfaces. The model suggests the switchover took place in the late 1980s at 400 K. The rapid HCl formation has been observed at 460 K within the Antarctic vortex later in the season [*Douglass et al.*, 1995]. (7) Chlorine nitrate hydrolysis is found to be important in maintaining high levels of ClO by recycling $ClONO_2$ back to Cl_x. The frequency of this reaction is a function of the frost point temperature, which is determined by the amount of water vapor in the vortex and ultimately by our initialization scheme. Reduction of vortex water vapor reduces ClO and the total amount of ozone loss. However, the reduction in water vapor is likely associated with significant denitrification which in turn suppresses $ClONO_2$ reformation by reducing the availability of NO_2. When HNO_3 and $ClONO_2$ are reduced along with water vapor, ozone loss is increased. Thus the model ozone loss does not appear overly sensitive to the initialization provided initial dehydration and denitrification are not arbitrarily specified. (8) Doubling 1992 Cl_y creates a larger ozone hole that has more ozone loss but one still constrained by the Antarctic vortex. All of the ozone disappears at both 400 and 440 K by September 17 under the doubling scenario shifting

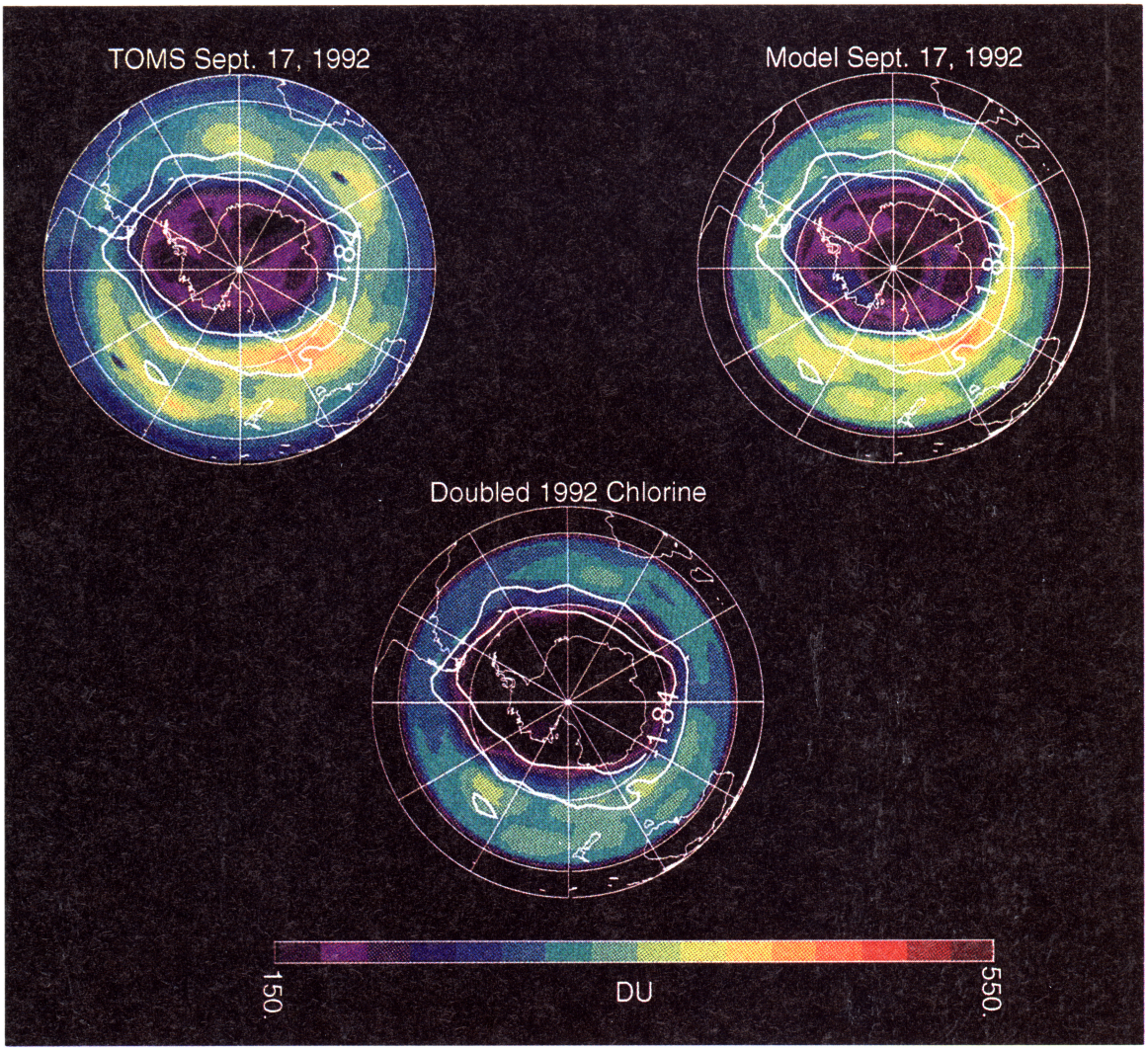

Plate 4. Comparison of 1992 TOMS, the 1992 model total ozone, and the 1992 model with doubled chlorine. The thin white lines show the 440-K main vortex edge and outer vortex edge from potential vorticity using the *Nash et al.* [1996] algorithm.

most of Cl_y into HCl. The high levels of chlorine in this case lead to substantial ozone loss outside the vortex region as well.

References

Anderson, J. G., D. W. Toohey, and W. H. Brune, Free radicals within the Antarctic vortex: The role of CFC's in Antarctic ozone loss, *Science*, *251*, 39–44, 1991.

Bowman, K. P., Large-scale isentropic mixing properties of the Antarctic polar vortex from analyzed winds, *J. Geophys. Res.*, *98*, 23,013–23,027, 1993.

Brasseur, G. P., Natural and anthropogenic perturbations of the stratospheric ozone layer, *Planet Space Sci.*, *40*, 403–412, 1992.

Chen, P., The permeability of the Antarctic vortex edge, *J. Geophys. Res.*, *99*, 20,563–20,572, 1994.

DeMore, W. B., S. P. Sander, D. M. Golden, R. F. Hampton, M. J. Kurylo, C. J. Howard, A. R. Ravishankara, C. E. Kolb, and M. J. Molina, Chemical kinetics and photochemical data for use in stratospheric modeling, in *Evaluation 11*, *NASA JPL Publ. 94-26*, 1994.

Dessler, A. E., et al., Correlated observations of HCl and ClONO2 from UARS and implications for stratospheric chlorine partitioning, *Geophys. Res. Lett.*, *22*, 1721–1724, 1995.

Douglass, A. R., et al., Interhemispheric differences in springtime production of HCl and $ClONO_2$ in the polar vortices, *J. Geophys. Res.*, *100*, 13,967–13,978, 1995.

Fahey, D. W., et al., Measurements of nitric oxide and total reactive nitrogen in the Antarctic stratosphere: Observations and chemical implications, *J. Geophys. Res.*, *94*, 16,665–16,682, 1989.

Hansen, D. R., and A. R. Ravishankara, Reactive uptake of $ClONO_2$ onto sulfuric acid due to reaction with HCl and H_2O, *J. Phys. Chem.*, *98*, 5728–5735, 1994.

Herman, J. R., et al., Meteor 3/total ozone mapping spectrometer observations of the 1993 ozone hole, *J. Geophys. Res.*, *100*, 2973–2983, 1995.

Hofmann, D. J., J. M. Rosen, J. W. Harder, and J. V. Hereford, Balloneborne measurements of aerosol condensation nuclei and cloud particles in the stratosphere at McMurdo Station, Antarctica, during spring 1987, *J. Geophys. Res.*, *94*, 11,253–11,269, 1989a.

Jones, R. L., et al., Lagrangian photochemical modeling studies of the 1987 Antarctic spring vortex, 1, Comparison with AAOE observations, *J. Geophys. Res.*, *94*, 11,529–11,558, 1989.

Kawa, S. R., et al., Photochemical partitioning of the reactive nitrogen and chlorine reservoirs in the high-latitude stratosphere, *J. Geophys. Res.*, *97*, 7905–7923, 1992.

Kawa, S. R., et al., Interpretation of NO_x/NO_y observations from AASE II using a model of chemistry along trajectories, *Geophys. Res. Lett.*, *20*, 2507–2510, 1993.

Kawa, S. R., et al., Activation of chlorine in sulfate aerosol as inferred from aircraft observations, *J. Geophys. Res.*, in press, 1996.

Kelly, K. K., et al., Dehydration in the lower Antarctic stratosphere

during late winter and early spring, 1987, *J. Geophys. Res.*, *94*, 11,317–11,358, 1989.

Lait, L. R., An alternative form of potential vorticity, *J. Atmos. Sci.*, *51*, 1754–1759, 1994.

Loewenstein, M., J. R. Podolske, K. R. Chan, and S. E. Strahan, Nitrous oxide as a dynamical tracer in the 1987 Airborne Antarctic Ozone Experiment, *J. Geophys. Res.*, *94*, 11,589–11,598, 1989.

Manney, G. L., et al., The evolution of ozone observed by UARS MLS in the 1992 late winter southern polar vortex, *Geophys. Res. Lett.*, *20*, 1279–1282, 1993.

Manney, G. L., et al., Lagrangian transport calculations using UARS data, I, Passive tracers, *J. Atmos. Sci.*, *52*, 3049–3068, 1995a.

Manney, G. L., R. W. Zurek, L. Froidevaux, J. W. Waters, A. O'Neill, and R. Swinbank, Lagrangian transport calculations using UARS data, II, Passive tracers, *J. Atmos. Sci.*, *52*, 3069–3081, 1995b.

McElroy, M. B., and R. J. Salawitch, Changing composition of the global stratosphere, *Planet Space Sci.*, *40*, 373–401, 1992.

McElroy, M. B., R. J. Salawitch, S. C. Wofsy, and J. A. Logan, Reductions of Antarctic ozone due to synergistic interactions of chlorine and bromine, *Nature*, *321*, 759–762, 1986.

McKenna, D. S., R. L. Jones, J. Austin, E. V. Browell, M. P. McCormick, A. J. Krueger, and A. F. Tuck, Diagnostic studies of the Antarctic vortex during the 1987 Airborne Antarctic Ozone Experiment: Ozone miniholes, *J. Geophys. Res.*, *94*, 11,641–11,668, 1989.

Molina, L. T., and M. J. Molina, Production of Cl_2O_2 from the self-reaction of the ClO radical, *J. Phys. Chem.*, *91*, 433–436, 1987.

Nash, E., P. A., Newman, J. E. Rosenfield, and M. R. Schoeberl, An objective determination of the polar vortex edge using Ertel's potential vorticity, *J. Geophys. Res.*, *101*, 9471, 1996.

Newman, P. A., et al., Meteorological atlas of the Southern Hemisphere lower stratosphere for August and September 1987, *NASA Tech. Memo. 4049*, 131 pp., 1988a.

Newman, P. A., L. R. Lait, and M. R. Schoeberl, The morphology and meteorology of southern hemisphere spring total ozone miniholes, *Geophys. Res. Lett.*, *15*, 923–926, 1988b.

Newman, P. A., R. Stolarski, M. R. Schoeberl, R. McPeters, and A. Krueger, The 1990 Antarctic ozone hole as observed by TOMS, *Geophys. Res. Lett.*, *18*, 661–664, 1991.

Peters, D., J. Egger, and G. Entzian, Dynamical aspects of ozone mini-hole formation, *Meteorol. Atmos. Phys.*, *5*, 205–214, 1995.

Prather, M. J., and E. E. Remsberg, The atmospheric effects of stratospheric aircraft: Report of the 1992 models and measurements workshop, *NASA RP-1292*, vols. 1–3, 1993.

Prather, M. P., and A. H. Jaffe, Global impact of the Antarctic ozone hole: Chemical propagation, *J. Geophys. Res.*, *95*, 3473–3492, 1990.

Proffitt, M. H., et al., A chemical definition of the boundary of the Antarctic ozone hole, *J. Geophys. Res.*, *94*, 11,437–11,448, 1989.

Redaelli, G., et al., UARS MLS O_3 soundings compared with LIDAR measurements using the conservative coordinates reconstruction technique, *Geophys. Res. Lett.*, *21*, 1535–1538, 1994.

Rosenfield, J. E., P. A. Newman, and M. R. Schoeberl, Computations of diabatic descent in the stratospheric polar vortex, *J. Geophys. Res.*, *99*, 16,677–16,689, 1994.

Schoeberl, M. R., and D. L. Hartmann, The dynamics of the stratospheric polar vortex and its relation to the springtime ozone depletions, *Science*, *251*, 46–52, 1991.

Schoeberl, M. R., and L. R. Lait, Conservative coordinate transformations for atmospheric measurements, *in The Use of EOS for Studies of Atmospheric Physics*, edited by G. Visconti and J. Gille, pp. 419–430, North-Holland, New York, 1992.

Schoeberl, M. R., and L. A. Sparling, Trajectory modeling, in *Diagnostic Tools in Atmospheric Physics*, edited by G. Fiocco and G. Visconti, IOS Press, Amsterdam, 1995.

Schoeberl, M. R., L. R. Lait, P. A. Newman, J. E. Rosenfield, The structure of the polar vortex, *J. Geophys. Res.*, *97*, 7859–7882, 1992.

Schoeberl, M. R., et al., The evolution of ClO and NO along air parcel trajectories, *Geophys. Res. Lett.*, *20*, 2511–2514, 1993a.

Schoeberl, M. R., R. S. Stolarski, A. R. Douglass, P. A. Newman, L. R. Lait, J. W. Waters, L. Froidevaux, and W. G. Read, MLS ClO observations and Arctic polar vortex temperatures, *Geophys. Res. Lett.*, *20*, 2861–2864, 1993b.

Solomon, S., Antarctic ozone: Progress toward a quantitative understanding, *Nature*, *347*, 347–354, 1990.

Stimpfle, R. M., et al., The response of ClO radical concentrations to variations in NO_2 radical concentrations in the lower stratosphere, *Geophys. Res. Lett.*, *21*, 2543–2546, 1994.

Stolarski, R. S., A. J. Krueger, M. R. Schoeberl, R. D. S. McPeters, P. A. Newman, and J. C. Alpert, Nimbus 7 SBUV/TOMS measurements of the springtime Antarctic ozone decreases, *Nature*, *322*, 308–311, 1986.

Thomason, W. L., and L. R. Poole, Use of stratospheric aerosol properties as diagnostic of Antarctic vortex process, *J. Geophys. Res.*, *98*, 23,003–23,012, 1993.

Toohey, D. W., et al., The seasonal evolution of reactive chlorine in the northern hemisphere stratosphere, *Science*, *261*, 1134–1136, 1993.

Toon, G. C., et al., Infrared aircraft measurements of stratospheric composition over Antarctica during September 1987, *J. Geophys. Res.*, *94*, 16,571–16,596, 1989.

Torres, O., Z. Ahmad, and J. R. Herman, Optical effects of polar stratospheric clouds on the retrieval of TOMS total ozone, *J. Geophys. Res.*, *97*, 13,015–13,024, 1992.

Waters, J. W., et al., Validation of UARS MLS ClO measurements, *J. Geophys. Res.*, *101*, 10,091–10,127, 1996.

Webster, C. R., et al., Chlorine chemistry on polar stratospheric cloud particles in the Arctic winter, *Science*, *261*, 1130–1134, 1993.

Wofsy, S. C., R. J. Salawich, J. H. Yatteau, M. B. McElroy, B. W. Gandrud, J. E. Dye, and D. Baumgardner, Condensation of HNO_3 on falling ice particles: Mechanism for dentrification of the polar stratospheres, *Geophys. Res. Lett.*, *17*, 449–452, 1990.

Woodbridge, E. L., et al., Estimates of total organic and inorganic chlorine in the lower stratosphere form in situ and flask measurements during AASE II, *J. Geophys. Res.*, *100*, 3057–3064, 1995.

World Meteorological Organization (WMO), Scientific assessment of ozone depletion: 1989, Global Ozone Research and Monitoring Project, *WMO Rep. 20*, Geneva, 1989.

World Meteorological Organization (WMO), Scientific assessment of ozone depletion: 1991, Global Ozone Research and Monitoring Project, *WMO Rep. 25*, Geneva, 1991.

World Meteorological Organization (WMO), Scientific assessment of ozone depletion: 1994, Global Ozone Research and Monitoring Project, *WMO Rep. 37*, Geneva, 1995.

A. E. Dessler, A. R. Douglass, S. Randolph Kawa, Paul A. Newman, M. R. Schoeberl, and R. S. Stolarski, NASA Goddard Space Flight Center, Mail Code 916, Greenbelt, MD 20771.

A. E. Roche, Lockheed Palo Alto Research Laboratory, Palo Alto, CA 94304.

J. M. Russell III, NASA Langley Research Center, Hampton, VA 23681.

J. W. Waters, Jet Propulsion Laboratory, Pasadena, CA 91109.

(Received January 3, 1996; revised May 18, 1996;
accepted May 31, 1996.)